Accepted Manuscript

Viscoelastic behavior of a novel aluminum metal matrix composite and comparison with pure aluminum, aluminum alloys, and a composite made of Al–Mg–Si alloy reinforced with SiC particles

Jose I. Rojas, Bathula Venkata Siva, Kanai Lal Sahoo, Daniel Crespo

PII: S0925-8388(18)30544-9

DOI: 10.1016/j.jallcom.2018.02.103

Reference: JALCOM 44979

To appear in: *Journal of Alloys and Compounds*

Received Date: 15 November 2017

Revised Date: 8 February 2018

Accepted Date: 9 February 2018

Please cite this article as: J.I. Rojas, B.V. Siva, K.L. Sahoo, D. Crespo, Viscoelastic behavior of a novel aluminum metal matrix composite and comparison with pure aluminum, aluminum alloys, and a composite made of Al–Mg–Si alloy reinforced with SiC particles, *Journal of Alloys and Compounds* (2018), doi: 10.1016/j.jallcom.2018.02.103.

Viscoelastic behavior of a novel aluminum metal matrix composite and comparison with pure aluminum, aluminum alloys, and a composite made of Al–Mg–Si alloy reinforced with SiC particles

Jose I. Rojas[a], Bathula Venkata Siva[b], Kanai Lal Sahoo[c] and Daniel Crespo[d]

[a] Department of Physics – Division of Aerospace Engineering, Universitat Politècnica de Catalunya; c/ Esteve Terradas 7, 08860, Castelldefels (Spain); corresponding author: email: josep.ignasi.rojas@upc.edu; phone: +34 93 413 4130; fax: +34 93 413 7007

[b] Department of Mechanical Engineering, Narasaraopeta Engineering College; Narasaraopet, Andhra Pradesh, 522601 (India); email: venkatasivanec@gmail.com

[c] Council of Scientific and Industrial Research (CSIR), National Metallurgical Laboratory; Jamshedpur, Jharkhand, 831007 (India), email: klsah@nmlindia.org

[d] Department of Physics, Universitat Politècnica de Catalunya; c/ Esteve Terradas 7, 08860, Castelldefels (Spain); email: daniel.crespo@upc.edu; phone: +34 93 413 4141, fax: +34 934 137 007

Abstract

The viscoelastic response of a novel composite (A356 aluminum alloy matrix with ceramic reinforcement particles developed from colliery shale waste) is measured with dynamic-mechanical analyzer, and is compared to pure aluminum, aluminum alloys A356, 7075 and 2024, and another composite (6061 aluminum alloy matrix reinforced with SiC particles). The studied materials show some common features but the novel composite is one of the most stable (a rapid decrease in stiffness starts only at very high temperature). Moreover, compared to the A356 alloy, the composite shows higher stiffness (since the reinforcement particles are stiffer than the A356 matrix and may foster precipitation hardening) and higher mechanical damping/internal friction (likely due to relaxations associated with the reinforcement particles and to the larger grain size for the A356 alloy). A typical relaxation peak in aluminum attributed to grain boundary sliding is suppressed in the composite because the reinforcement particles pin the grain boundaries.

Keywords metal matrix composites; grain boundaries; mechanical properties; microstructure; optical spectroscopy; scanning electron microscopy, SEM

1. INTRODUCTION

The use of metal matrix composites (MMC) has increased steadily in the last decades. Conventional MMC are usually produced by addition of either Al_2O_3 or SiC particles, or their combinations, into molten pure metals or alloys. However, when preparing the MMC through melting routes like stir casting method, there is significant loss of those costly particles. This is due to poor wettability of the particles in the melt and due to the density difference between the particles and the matrix. These waste of particles makes fabrication more expensive [1]. Several works highlight the importance of lightweight MMC and urge researchers to develop cheaper production techniques. In this research, a novel aluminum metal matrix composite (AMC) with A356 aluminum alloy matrix was produced with an innovative technique that allows incorporating reinforcement consisting of Al_2O_3, SiC and C, novel ceramic particles developed indigenously from colliery shale (CS). CS is a waste obtained during mining of coal from underground mines, for which the essential constituents are Al_2O_3, SiC, SiO_2 and C. The purpose of using the proposed fabrication procedure was to obtain a cost-effective AMC, and this is achieved thanks to the fact that the proposed technique avoids addition of costly reinforcing agents like Al_2O_3 or SiC [1].

Some of the mechanical properties of this novel AMC have been reported in previous works [2,3]. Particularly, the new AMC was compared with another composite prepared with SiC. In these investigations, SiC particles were used as reinforcement because of their attractive properties like high hardness, strength and good resistance to thermal shock, compared to Al_2O_3, TiC, etc. However, the viscoelastic response of this AMC has not been studied yet. Thus, the objective of this research is to characterize the influence of the temperature, loading frequency and microstructure on the viscoelastic behavior of this novel, low-cost AMC, and compare it with that reported for pure aluminum [4,5] and commercial, age-hardenable aluminum alloys (AA) 7075 (Al–Zn–Mg) and 2024 (Al–Cu–Mg) [6,7], and another AMC made of AA 6061 (Al–Mg–Si) matrix and SiC particles [8]. Studying the viscoelastic behavior of materials, a consequence of mechanical relaxation phenomena under dynamic loading, is interesting because it offers an alternative method for analyzing the microstructure and enables a deeper understanding of properties like mechanical damping and yielding [9], and ultimately fatigue, because metals are subjected to dynamic loading in most structural applications.

This research will thus help establish the interest of such novel, low-cost AMC for applications like, for instance, damping systems, compared to other considered materials, some of which show excellent mechanical properties and due to this are suitable for a number of industrial applications, e.g., in the aerospace sector and transport industry. In particular, the principal conclusions of this investigation are that the novel AMC is one of the most stable materials, retaining high stiffness up to very high temperature, and that the AMC shows higher stiffness and higher mechanical damping than the A356 matrix alloy.

1.1 Modelling of viscoelastic response

The dynamic-mechanical behavior of viscoelastic solids can be described using either the complex compliance approach or the complex modulus approach. In the former case, for a solid showing a single relaxation process, the Debye equations are [9]:

$$J_1(T,\Omega) = J_u + \frac{\delta J}{1+(\Omega\tau)^2} \qquad \textbf{Eq. 1}$$

$$J_2(T,\Omega) = \delta J \frac{\Omega\tau}{1+(\Omega\tau)^2} \qquad \textbf{Eq. 2}$$

where J_1 and J_2 are, respectively, the real and imaginary parts of the complex compliance J, $J_u(T)$ is the unrelaxed compliance (i.e., J for $\Omega \to \infty$), $\delta J(T) = J_r - J_u$ is the relaxation of the compliance, $J_r(T)$ is the relaxed compliance (i.e., J for $\Omega \to 0$), $\Omega = 2\pi f$ is the angular loading frequency, and $\tau(T)$ is the average or main mechanical relaxation time of the relaxation process occurring at a given temperature. When the rate-limiting step of the considered relaxation is that of movement over an energy barrier, which is often valid, the relaxation rate $1/\tau(T)$ exhibits Arrhenius-type temperature dependence [10,11]:

$$\frac{\mathbf{1}}{\boldsymbol{\tau}} = \frac{\mathbf{1}}{\boldsymbol{\tau_0}}\mathbf{exp}\left(-\frac{\boldsymbol{E_A}}{\boldsymbol{k_B T}}\right) \qquad \textbf{Eq. 3}$$

where $1/\tau_0$ is the pre-exponential coefficient, E_A is the activation energy associated with the relaxation process, and k_B is the Boltzmann constant. On the other side, in the complex modulus approach, the viscoelastic behavior is described using the following equations:

$$E'(T,\Omega) = E'' \frac{J_1}{J_2} \qquad \textbf{Eq. 4}$$

$$E''(T,\Omega) = \frac{J_2}{{J_1}^2+{J_2}^2} \qquad \textbf{Eq. 5}$$

where E' and E" are, respectively, the real and imaginary parts of the dynamic Young's modulus E. The storage modulus E' is the elastic component of E, which accounts for the deformation energy stored by the material, while the loss modulus E" is the viscous component of E, which accounts for the energy dissipation due to internal friction (IF) associated with mechanical relaxation phenomena. From Eq. 1, 2 and 5, it follows that the time-temperature relaxation spectrum for Debye peaks can be expressed as [9]:

$$\boldsymbol{E"(T,\Omega) = \delta E(\Omega\tau/(1 + (\Omega\tau)^2))} \qquad \textbf{Eq. 6}$$

where $\delta E(T) = E_u - E_r$ is the relaxation of the dynamic modulus, $E_u(T) = 1/J_u$ is the unrelaxed modulus (i.e., E for $\Omega \to \infty$), and $E_r(T) = 1/J_r$ is the relaxed modulus (i.e., E for $\Omega \to 0$). Indeed, relaxation processes are usually characterized from the analysis of E". Particularly, E" peaks are defined mainly by four characteristics: the intensity of the peak, the bluntness or broadness of the peak, and the power laws defining the low- and high-frequency tails [11]. If the broadness of the peak is larger than that of a Debye peak, this is associated with existence of a distribution of relaxation times, which occurs if we have several coupled or overlapping relaxations, or a single relaxation with a spectrum of activation energies. That is, in this approach, the shape of E" describes the influence of the relaxation time spectrum, i.e., the deviation from a Debye process [11]. In crystalline metals, classical anelastic relaxation phenomena are restricted to a small volume, e.g., defects like grain boundaries and dislocations [9]. Because of this, relaxations in these materials do not usually have large magnitudes, and the peaks are then usually close to a Debye relaxation.

2. MATERIALS AND METHODS

For the preparation of the novel AMC, aluminum of 99.6% purity was used with reinforcement particles from freshly prepared ceramic composite from CS [1,12]. The chemical composition of CS consists mainly of SiC (obtained by reacting SiO_2 with C with plasma synthesis), and then Al_2O_3 and C. The measured size distribution of the CS powder after plasma synthesis can be seen in Fig. 5 in [1]. As can be seen, the particle dimensions range from around 20 nm to 200 μm. Furthermore, the powder was sieved such that the particles finally added in the novel AMC had sizes ranging from 20 nm to 40 μm. A pit-type melting furnace with bottom pouring facility was used. An adequate amount of reinforcement particles was preheated at 873 ± 5 K (600 ± 5ºC) for enhancing wettability before being added to the melt. During the melting process, the furnace, with Argon atmosphere, was set at a

controlled temperature of 1073 ± 5 K (800 ± 5ºC). The molten metal was stirred with a BN-coated stainless steel rotor, with rotating speed of 600-700 rpm. To further improve the wettability of the particles, 0.5 wt.% Mg was added to the melt. The reinforcement material preheated *in-situ* was poured in the center of a vortex created in the melt due to stirring. The rotor was pushed down slowly keeping a clearance gap of 12 mm with the bottom. The rotor was then pushed back slowly to its initial position. The liquid pouring temperature was 973 ± 5 K (700 ± 5ºC). The melt was finally cast into a mold pre-heated at 573 K (300ºC).

A Q800 dynamic-mechanical analyzer (DMA) from TA Instruments (New Castle, DE, USA) was used to measure the viscoelastic response of the AMC in N_2 atmosphere. The DMA records the storage modulus E', the loss modulus E'' and the loss tangent (i.e., the ratio E''/E'), also termed mechanical damping or $\tan\delta$. The 3-point bending clamp was used, with length between unmovable supports of 50 mm and preload force of 0.10 N, and the DMA was set to sequentially apply dynamic loading with frequencies from 0.01 to 100 Hz, at temperatures from 308 to 873 K (35 to 600ºC) in step increments of 10 K (for an average heating rate of ≈0.10 $K \cdot min^{-1}$). In general, all the samples yielded above the maximum tolerance threshold of the DMA before reaching 873 K (600ºC), thus leading to a premature interruption of the test, after which the samples were cooled by air quenching.

The specimens of Al–Zn–Mg and Al–Cu–Mg alloys for DMA were prepared from sheet of as-received, commercial AA 7075-T6 and 2024-T3. The T6 temper consists in solution heat-treatment at 753 K (480ºC) for 1 h, followed by rapid water quenching to room temperature (RT) and artificial aging at 393 K (120ºC) for 24 h. The T3 temper consists also in solution heat-treatment, followed by rapid water quenching to RT, cold-working and natural ageing. Table 1 and Table 2 show, respectively, the mechanical properties and compositions in wt.% and at.% for the as-received alloys, as given by the provider, Alu-Stock, S.A. (Vitoria-Gasteiz, Spain). A first couple of sets of specimens (termed AA 7075-T6 and 2024-T3, from now on) were machine cut from the as-received alloys to rectangular plates 60 mm long, 10 mm wide and 2 mm thick. Two more sets of identical plates (termed AA 7075 and 2024, from now on) were solution heat-treated to remove the T6 and T3 temper, respectively, rapidly quenched in water to RT, and tested in the DMA immediately after.

The pure aluminum specimens for DMA were prepared from as-received sheet in the H24 temper with 99.5 wt.% purity according to Alu-Stock, S.A. The H24 temper consists in cold-

working beyond desired hardness, followed by a softening treatment consisting in annealing up to halfway of peak hardness. The specimens were machine cut to rectangular plates with dimensions equal to those mentioned above. To remove the H24 temper, the specimens were annealed at 753 K (480ºC) for 30 min, and immediately quenched in water to RT.

Table 1 Mechanical properties of the studied materials.

Material	Yield stress [MPa]	UTS [MPa]	Ductility	Brinell Hardness
AA 7075-T6	502	583	12% area reduction	HB 161
AA 2024-T3	377	485	15% area reduction	HB 123
A356	230	290	13% elongation	-
Novel AMC	-	260	8.9% elongation	-

Table 2 Chemical composition of the as-received, commercial aluminum alloys 7075-T6, 2024-T3 and A356.

Aluminum alloy	Units	Si	Fe	Cu	Mn	Mg	Zn	Ti	Cr	Al
AA 7075-T6	wt.%	0.06	0.15	1.50	0.01	2.58	6.00	0.05	0.19	89.46
	at.%	0.06	0.08	0.67	0.01	2.99	2.59	0.03	0.10	93.48
AA 2024-T3	wt.%	0.18	0.28	4.46	0.64	1.35	0.04	0.05	0.01	92.98
	at.%	0.18	0.14	1.95	0.32	1.54	0.02	0.03	0.01	95.81
A356	wt.%	6.50	0.12			0.45				92.93
	at.%	6.26	0.06			0.50				93.18

For DMA also, rectangular plates with dimensions equal to those mentioned above were machine cut from ingots of A356 alloy and the novel AMC. More details on the studied material and experimental set up can be found for pure aluminum in [4,5], for AA 7075 and 2024 in [13], for AA 6061 reinforced with SiC particles in [8], and for the A356 alloy and the novel AMC in [1,12]. The latter two materials were also analyzed with optical microscope. Metallographic samples were cut into ≈1×1 cm^2 from the central part of the ingot and polished using belt polishing and emery paper from coarser to finer ranges. After that, cloth polishing was applied using fine Al_2O_3 powder. The samples were then polished with Silvo solution, consisting of iso-propyl alcohol, ammonium hydroxide and SiO_2 powder, which was used for cleaning and suspending the tarnish on surfaces and also to protect from oxidation [12]. Finally, the samples were etched with Keller's reagent [14]. From the micrographs, the average grain size was measured. Particularly, each average was obtained from at least four micrographs (i.e., from a total analysis area of 0.172 mm^2).

The samples of A356 alloy and the novel AMC were taken for examination with a scanning electron microscope (SEM). The AMC samples were further analyzed with energy-dispersive

X-ray (EDX) spectroscopy. Both analyses were conducted with a SEM Hitachi S 3400 N, with attached EDX spectroscopy equipment. The SEM specifications are as follows: resolution of 3 nm in high-vacuum mode; chamber capable of accommodating specimens with lengths up to 254 mm, 5-axis computer controlled motorized stage [12]. Finally, the surface morphology of the AMC samples was analyzed with atomic force microscope (AFM). The AFM was 5000 Hitachi High-Tech Science Corp., Version 6.04. Particularly, the samples were analyzed with viscoelastic dynamic force microscope (VE-DFM), i.e., in non-contact mode.

3. RESULTS AND DISCUSSION

3.1 Storage modulus

Fig. 1 shows *E'* for all the tested frequencies for A356 aluminum alloy and the novel AMC. Fig. 2 shows *E'* for 1 Hz for the former materials, pure aluminum [4,5], Al–Zn–Mg and Al–Cu–Mg alloys [4,6,7], and another AMC made of AA 6061 matrix and SiC particles [8].

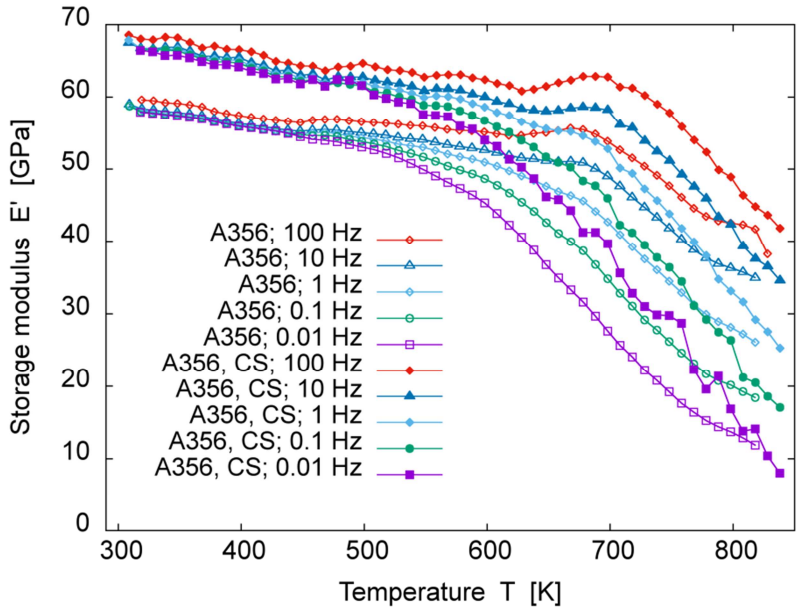

Fig. 1 Storage modulus *E'* vs. temperature *T* from DMA at frequencies ranging from 0.01 to 100 Hz, for A356 aluminum alloy and a novel composite made of A356 alloy matrix with reinforcement particles from colliery shale (CS).

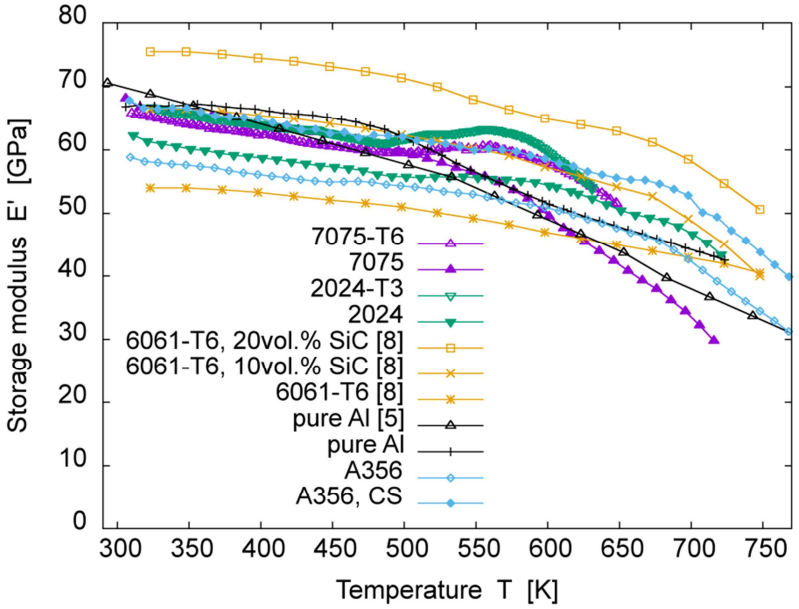

Fig. 2 Storage modulus *E'* vs. temperature *T* from DMA at frequency of 1 Hz, for A356 aluminum alloy, a novel composite made of A356 alloy matrix with reinforcement particles from colliery shale (CS), pure aluminum, Al–Zn–Mg and Al–Cu–Mg alloys, and a composite made of AA 6061 matrix and SiC particles.

The DMA measurements may differ noticeably from test to test due to instrument error, imperfections of the samples or errors in measuring their dimensions, etc. Bearing this in mind, the results in Fig. 1 and Fig. 2 for the various materials are qualitatively similar in most cases and show some common features that were discussed in [4,6,7,13]. The novel AMC shows higher stiffness than the A356 alloy matrix (see Fig. 1). This is expected from the rule of mixtures, since the embedded reinforcement particles (Al_2O_3, SiC and C particles) are stiffer than the matrix, and because embedded particles usually foster precipitation hardening. For instance, the same occurs for the composite made of AA 6061 matrix and SiC particles, compared to AA 6061 alone, as shown in Fig. 2 [8]. From this figure also, the stiffness of the A356 alloy and the novel AMC seems comparable to the other materials. While for pure aluminum *E'* starts to decrease significantly at 473 K (200ºC), for the A356 alloy this phenomenon occurs at higher temperature, around 623 K (350ºC), and even later for the novel AMC (i.e., the latter is the most stable). This may also be due to a stabilizing effect by the reinforcement particles.

3.2 Loss modulus

Fig. 3 shows *E"* for all the tested frequencies for A356 aluminum alloy and the novel AMC. Fig. 4 shows *E"* for 1 Hz for the former materials, pure aluminum [4], Al–Zn–Mg and Al–Cu–Mg alloys [4,6,7], and another AMC made of AA 6061 matrix and SiC particles [8].

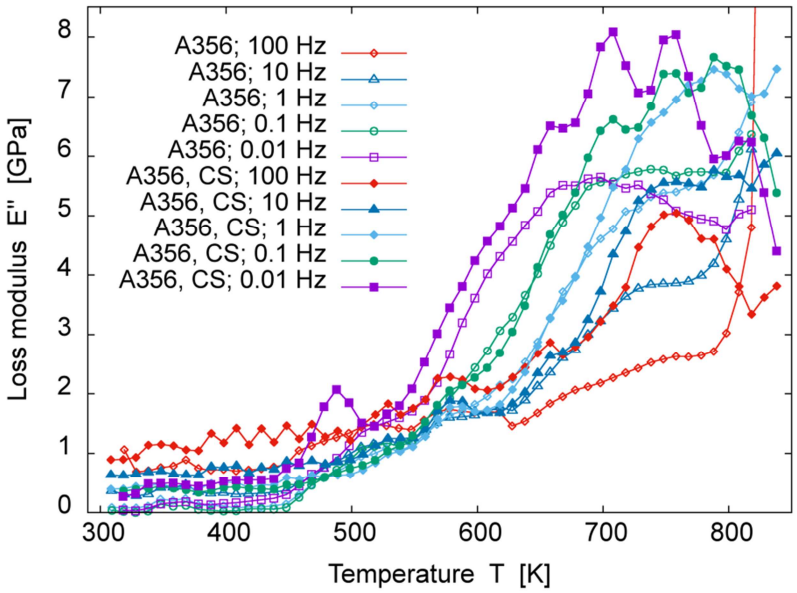

Fig. 3 Loss modulus *E″* vs. temperature *T* from DMA at frequencies ranging from 0.01 to 100 Hz, for A356 aluminum alloy and a novel composite made of A356 alloy matrix with reinforcement particles from colliery shale (CS).

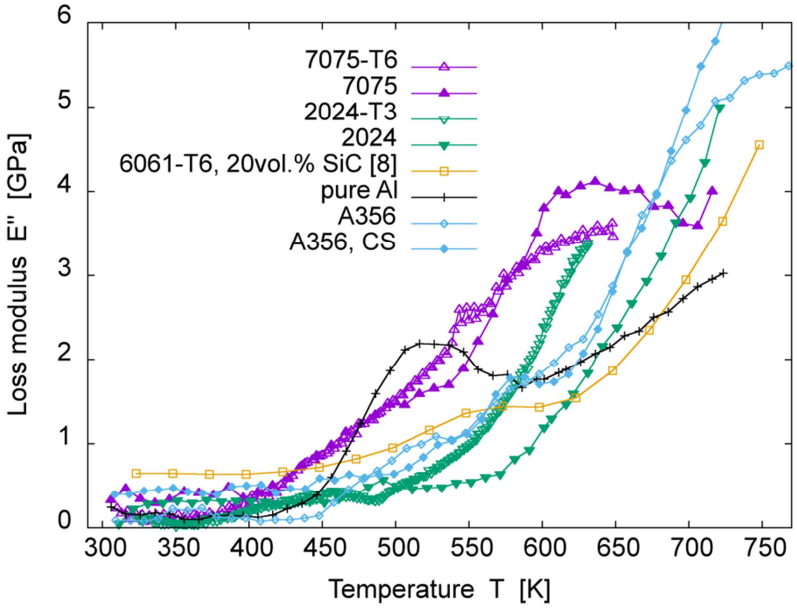

Fig. 4 Loss modulus *E″* vs. temperature *T* from DMA at frequency of 1 Hz, for A356 aluminum alloy, a novel composite made of A356 alloy matrix with reinforcement particles from colliery shale (CS), pure aluminum, Al–Zn–Mg and Al–Cu–Mg alloys, and a composite made of AA 6061 matrix and SiC particles.

The behavior of *E*" for most of these materials is again qualitatively similar and shows features that were discussed thoroughly in [4,6,7,13]. Moreover, the mechanical damping/ internal friction exhibits qualitatively the same behavior as *E*". To avoid redundancy, these

measurements are not shown in this work, but the following explanations for E'' also apply to the damping behavior.

At low temperature, E'' shows no significant changes with temperature. Then, a rapid increase of E'' starts at ≈423–523 K (150–250ºC). In many cases, this growth is monotonical, reaching very high values without showing a peak. The E'' peaks shown by AA 7075, A356 alloy and the novel AMC at ≈648–748 K (375–475ºC) are probably caused by the prolonged ageing at high temperature, which may ultimately result in a decrease of E'' due to precipitate dissolution [9]. Monotonical growth of E'' is usually explained by the high-temperature IF background, roughly exponential with temperature for most materials [15,16], and by presence of coupled or overlapping relaxations [9,15,16]; namely, a classical E'' peak in polycrystalline aluminum at ≈503–603 K (230–330ºC), typically attributed to grain boundary sliding (GBS) [9,15] and more recently to other diffusion-controlled processes like dislocation climb [16]. For the alloys, relaxation peaks associated with precipitates may also be contributing to the E'' growth. Finally, there is a contribution by the linear thermoelastic background, proportional to the temperature, but it should not be very important in the studied frequency range [16].

The peak attributed to GBS, which has been observed in Al–Mg [15], Al–Zn–Mg and Al–Cu–Mg alloys [17,18], is clearly evident in our results for pure aluminum at ≈523 K (250ºC), as shown in Fig. 4. Conversely, it cannot be distinguished for the other considered materials and particularly the A356 alloy and the novel AMC. Pinning of grain boundaries by precipitates and/or reinforcement particles, preventing the boundaries from sliding, may explain why this peak is suppressed for these materials. Namely, suppression of GBS has already been associated with presence of β phase in Al–Mg alloys [15] and presence of large particles at the grain boundaries in AA 7075 [14]. Finally, the novel AMC shows higher E'' than the A356 alloy matrix, particularly at high temperatures, i.e., above 523 K (250ºC). This is likely due to IF phenomena associated with the embedded reinforcement particles and other reasons explained later on. Both materials show higher E'' than pure aluminum only above 598 K (325ºC), i.e., a bit over the temperature at which the latter shows the GBS peak.

The E'' results were processed to obtain the activation parameters of the thermally activated E'' peaks. Particularly, E_A and τ_0 can be computed from the temperature- or frequency-shift of the peaks. However, as shown in Fig. 4, some of the peaks are not fully captured and/or it is

difficult to establish their position. In this case, an alternative to obtain the activation parameters for the relaxation(s) responsible for the peaks is to analyze their tails, following a process discussed in [11,13,19]. Namely, Eq. 6 shows that, for a given value of $\Omega\tau$, E'' is the same regardless the value of the frequency or Ω. Hence, for each curve corresponding to a different frequency in Fig. 3, the temperature for a given value of E'' (i.e., a given value of $\Omega\tau$) can be obtained. With these data, Arrhenius plots can be drawn, as derived from Eq. 3, where: $\ln(\Omega) = \ln(\Omega\tau) - \ln(\tau_0) - E_A/k_BT$. Since the value of $\Omega\tau$ is given, E_A and τ_0 can be estimated from the linear regressions of these Arrhenius plots.

Using this procedure, plots like those shown in Fig. 5 were obtained for the region of growth of E'', from which we estimated the activation parameters for this region. In particular, this procedure was done with four different values of E'': 2800, 3000, 3100 and 3200 MPa for the A356 alloy and 3000, 3200, 3400 and 3600 MPa for the novel AMC. For the four cases for each material, the variations in the computed E_A respect to the average E_A were below 3.75%, showing the robustness and precision of the method. Particularly, for the A356 alloy, $E_A =$ 1.80 ± 0.02 eV/atom and $\tau_0 = (4.03 \pm 1.33) \times 10^{-15}$ s, and, for the AMC, $E_A = 2.41 \pm 0.08$ eV/atom and $\tau_0 = (2.50 \pm 2.13) \times 10^{-19}$ s (the values for AA 7075 and 2024 were presented in [13]). These values correspond neither to the relaxation associated with GBS in aluminum, for which E_A is reported to be 1.48 eV/atom [9,15], nor to relaxations caused by dislocations, for which τ_0 usually ranges from 10^{-10} to 10^{-13} s [15]. Indeed, the computed activation parameters are similar to those reported by Golovin *et al.* [15] for a so-called P2 peak, and Yamaguchi *et al.* [16] inform about a diffusion-controlled loss peak in this temperature range.

Finally, when a material is subjected to dynamic loading, energy is dissipated due to IF. Most of this energy manifests as heat and causes a temperature increase in the material (a process termed hysteresis heating). Amiri and Khonsari [20] affirm that all metals, when subjected to hysteresis heating, are prone to fatigue. As shown in Fig. 3, E'' is higher for the novel AMC than for the A356 alloy for all the frequencies in the studied temperature range. Therefore, the hysteresis heating associated with IF should be more intense for the AMC. This suggests that this material should be more prone to fatigue than the A356 alloy. However, many other factors affect also the fatigue response of materials, and thus further research (e.g., fatigue tests of the AMC) would be necessary to clarify this point.

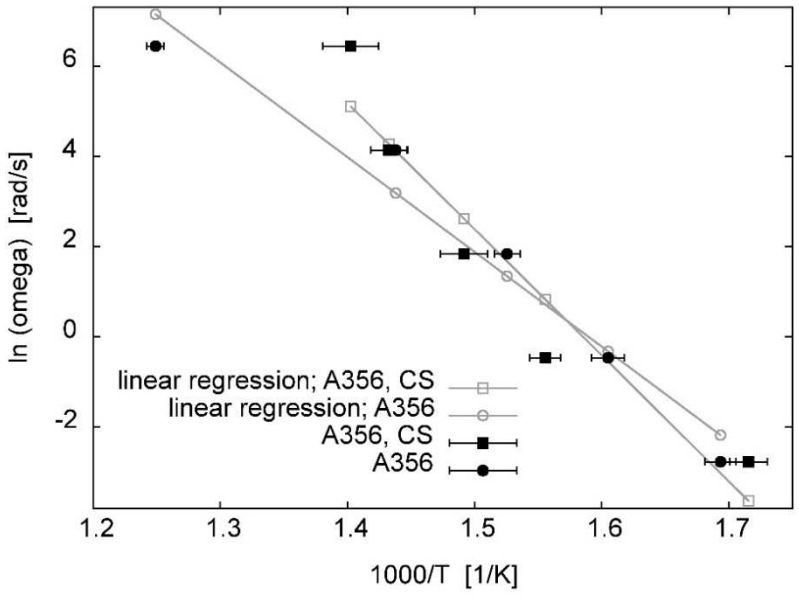

Fig. 5 Arrhenius plots showing the logarithm of the frequency vs. the reciprocal of the temperature for the tails of the peaks observed for A356 aluminum alloy and a novel composite made of A356 alloy matrix with reinforcement particles from colliery shale (CS).

3.3 Characterization of the microstructure

Fig. 6 and Fig. 7 show examples of bright-field optical micrographs obtained for A356 aluminum alloy and the novel AMC, respectively. From these optical micrographs, it appears that the grains are slightly stretched, rather than equiaxed, for both the A356 alloy and the novel AMC. The average grain size measured for the former material was 23.3 μm, while it was 14.5 μm for the novel composite. The larger grain size for the A356 alloy compared to the AMC is coherent with the lower E'' shown by the former, because 1) a coarser grain distribution means less grain boundary per unit volume, and thus less IF associated with GBS, and 2) the high-temperature IF background is inversely proportional to grain size [15]. This explains also why, at very high temperature, e.g., above 673 K (400ºC), E'' is higher for the A356 alloy and the novel AMC than for AA 7075 and 2024 [6,7], since the average grain size measured for the latter materials was 154.3 and 138.5 μm, respectively.

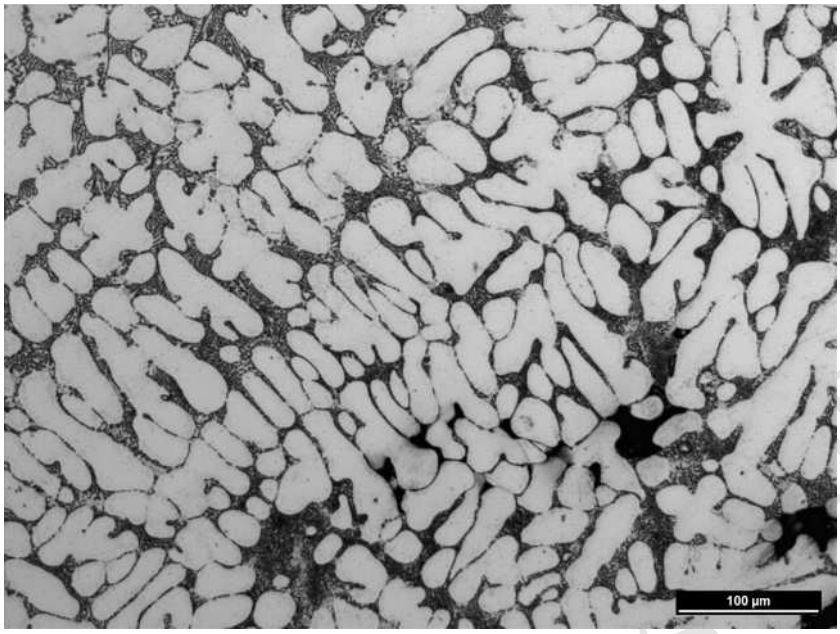

Fig. 6 Bright-field optical micrograph for A356 aluminum alloy.

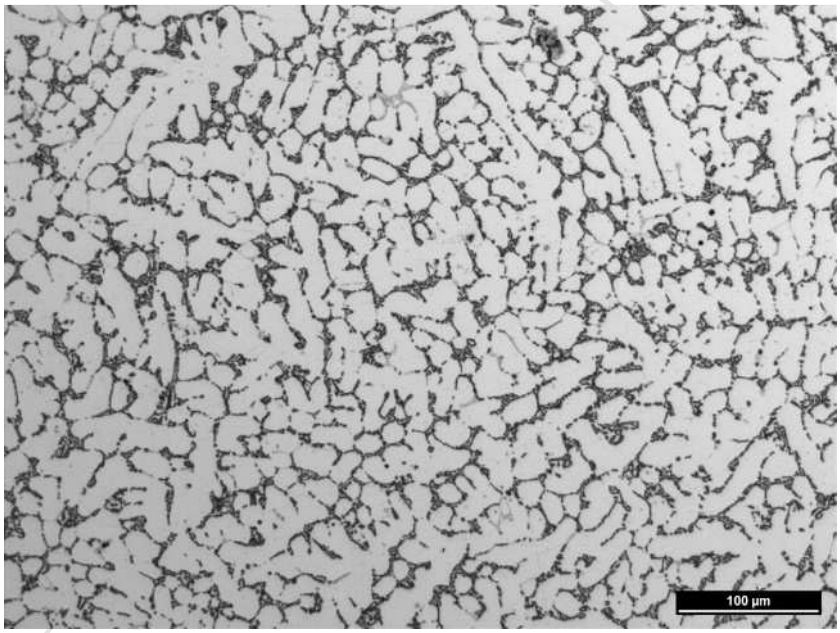

Fig. 7 Bright-field optical micrograph for the novel composite made of A356 alloy matrix with reinforcement particles from colliery shale.

Fig. 8 and Fig. 9 show examples of SEM images obtained for A356 aluminum alloy and for the novel AMC, respectively (more SEM images can be found as supplementary material). In general, composites like the novel AMC show smaller secondary dendrite arm spacing (SDAS) compared to alloys like the matrix alloy. Particularly, the smaller SDAS for the AMC is due to the CS particles that stimulated heterogeneous nucleation of the primary phase. It was observed that most of the particles segregated at the grain boundaries. During

solidification, the growth of primary phases pushes the particles toward the grain boundaries. The high surface tension due to large surface area-to-volume ratio at the interface and the small mass of the particles contribute to the agglomeration of the particles and their clustering at the grain boundaries. Grains are also not large owing to pinning of grains at the boundaries by incoherent particulates (i.e., grain boundary pinning by precipitates inhibits grain growth; this phenomenon has been observed in a variety of materials [21,22]).

Fig 10 shows examples of the AFM images obtained for the AMC (more images can be found as supplementary material) with VE-DFM. From the AFM and SEM images it is clear that, in general, the embedded reinforcement particles are not spheroidal but rather show irregular, non-equiaxed shapes. Moreover, the particles that can be seen in Fig. 9 (bottom) have dimensions ranging from around 15 nm to 500 nm. Finally, Table 3 shows the results on chemical compositions obtained with EDX for the AMC. Particularly, the EDX results provided in Table 3 correspond to the matrix and some of the particles observed in the SEM images included as supplementary material, like, for instance, a SiC particle, Si particle, and Silicide particle (β, Al_5FeSi).

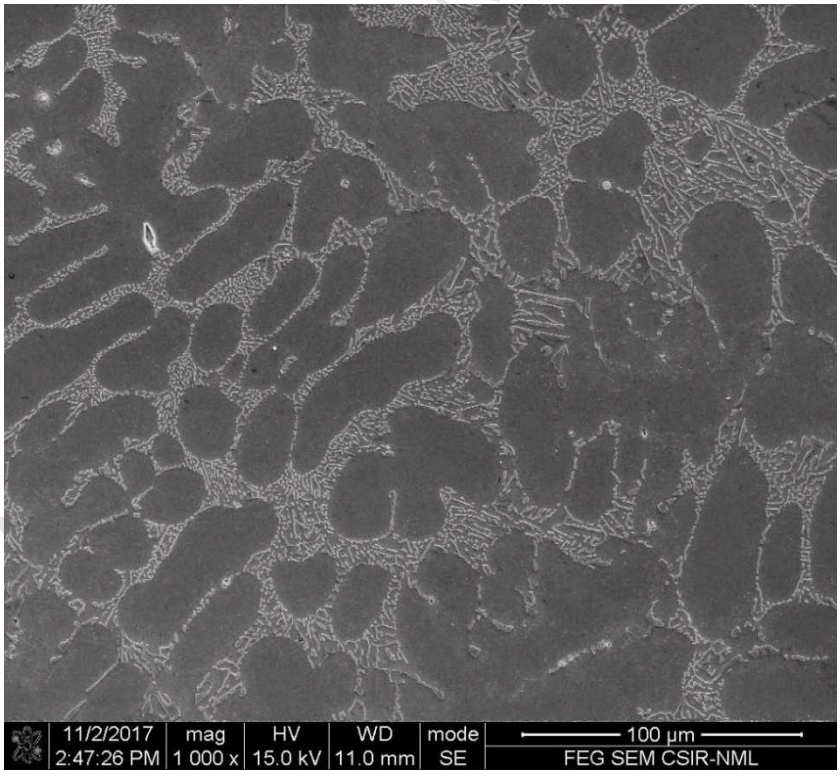

Fig. 8 SEM image for A356 aluminum alloy.

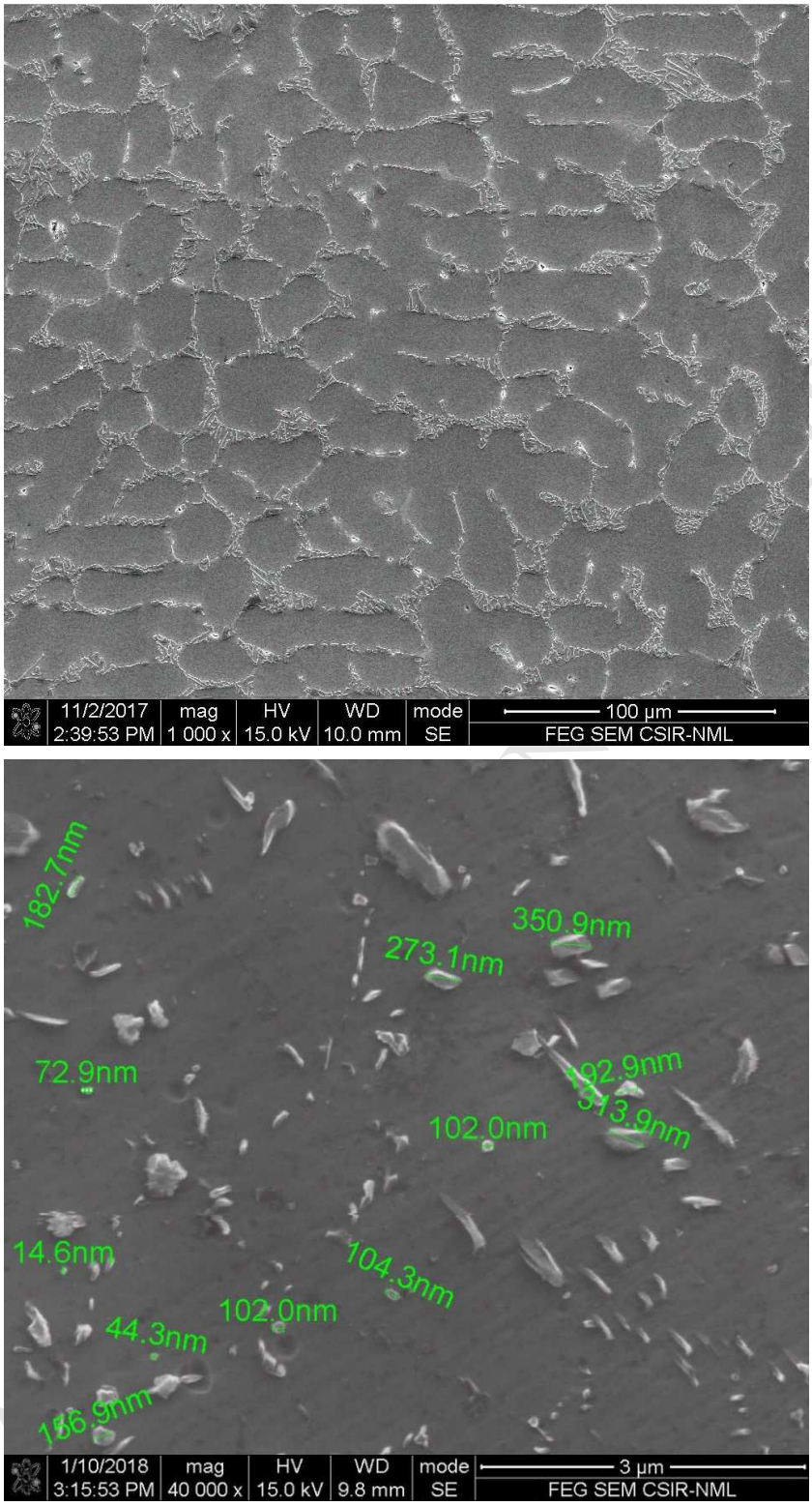

Fig. 9 SEM images for the novel composite made of A356 alloy matrix with reinforcement particles from colliery shale.

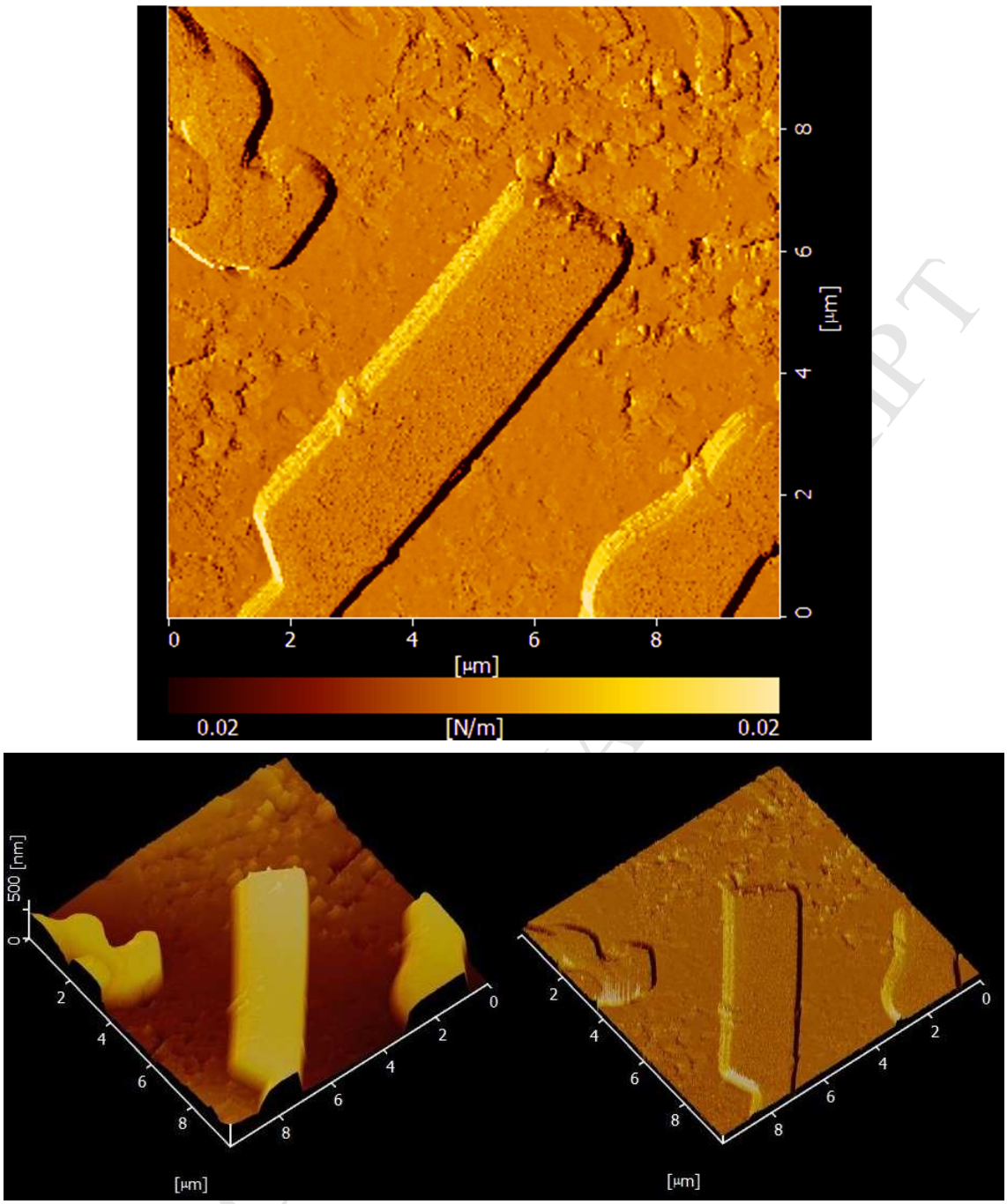

Fig. 10 Atomic force microscope (AFM) results in 2D view (top) and 3D view (bottom) for the novel composite made of A356 alloy matrix with reinforcement particles from colliery shale.

Table 3 Chemical compositions as obtained from energy-dispersive X-ray (EDX) spectroscopy for the novel aluminum metal matrix composite. Fig. A and B can be found in supplementary material.

Item	Units	Si	Fe	C	O	Mg	Al
Si particle	wt.%	97.41					2.59
(mark #1 in Fig. B)	at.%	97.31					2.69
Small, rectangular precipitate	wt.%	3.69	0.49	0.71	1.51	1.54	92.06
(mark #2 in Fig. B)	at.%	3.49	0.23	1.56	2.50	1.68	90.53
Silicide particle (β, Al_5FeSi)	wt.%	23.87	16.91			5.56	53.66
(mark #3 in Fig. B)	at.%	25.21	8.99			6.78	59.02
Irregular-shaped particle	wt.%	72.29	0.42			0.12	27.16
(mark #4 in Fig. B)	at.%	71.63	0.21			0.14	28.02
SiC particle	wt.%	48.16	0.66	8.13		0.61	42.44
(mark #5 in Fig. B)	at.%	42.86	0.29	16.92		0.63	39.30
Matrix	wt.%	0.82	0.44	6.86		0.75	91.13
(mark #6 in Fig. B)	at.%	0.72	0.20	14.22		0.77	84.09
Al–SiC composite	wt.%	39.29		2.91	0.79	2.31	54.71
(mark #1 in Fig. G)	at.%	36.69		6.35	1.29	2.49	53.18
Irregular-shaped particle	wt.%	81.41		2.84			15.75
(mark #2 in Fig. G)	at.%	77.95		6.36			15.70

4. CONCLUSIONS

After comparing the viscoelastic response of the novel AMC with that of pure aluminum, aluminum alloys A356, 7075 and 2024, and another composite made of AA 6061 matrix and SiC particles, the main conclusions are:

1. The storage modulus E', loss modulus E'' and mechanical damping of these materials show some common features that were already discussed thoroughly in [4,6,7,13].
2. The AMC is stiffer (shows higher E') than the A356 alloy matrix, because the reinforcement particles are stiffer than the A356 matrix and may foster precipitation hardening.
3. The rapid decrease of E' starts at higher temperature for the AMC compared to most of the considered materials, i.e., it is one of the most stable.
4. The typical relaxation peak in aluminum attributed to GBS is suppressed in the AMC, probably because the reinforcement particles and precipitates pin the grain boundaries.
5. Pure aluminum shows higher E'' and mechanical damping than the AMC and A356 alloy only for temperatures close to that where it shows the GBS relaxation peak.
6. The AMC shows higher E'' and mechanical damping than the A356 alloy, particularly above 523 K (250ºC). This may be due, on one hand, to the contribution by relaxations

associated with the reinforcement particles, and, on the other, to the larger grain size for the A356 alloy, because 1) a coarser grain distribution means less grain boundary per unit volume, and thus less IF associated with GBS, and 2) the high-temperature IF background is inversely proportional to grain size.

ACKNOWLEDGEMENTS

This work was supported by the Spanish MINECO [grant number FIS2014-54734-P] and the AGAUR from *Generalitat de Catalunya* [grant number 2014 SGR 581]. We thank also the valuable help by Mr. Chenyang Xie in preparing samples for DMA. Conflicts of interest: none.

REFERENCES

[1] S.B. Venkata Siva, K.L. Sahoo, R.I. Ganguly, R.R. Dash, S.K. Singh, B.K. Satpathy, G. Srinivasarao, Preparation of Alumimium metal matrix composite with novel in situ ceramic composite particles, developed from waste colliery shale material, Metall. Mater. Trans. B. 44B (2013) 800–808.

[2] S.B. Venkata Siva, R.I. Ganguly, G. Srinivasa Rao, K.L. Sahoo, Machinability of aluminum metal matrix composite reinforced with in-situ ceramic composite developed from mines waste, Mater. Manuf. Process. 28 (2013) 1082–1089. doi:10.1080/10426914.2013.811734.

[3] S.B. Venkata Siva, R.I. Ganguly, G. Srinivasa Rao, K.L. Sahoo, Wear behaviour of novel Al based composite reinforced with ceramic composite (Al2O3–SiC–C) developed from colliery shale material, Tribology. 8 (2014) 117–124. doi:10.1179/1751584X13Y.0000000050.

[4] J.I. Rojas, D. Crespo, Onset Frequency of Fatigue Effects in Pure Aluminum and 7075 (AlZnMg) and 2024 (AlCuMg) Alloys, Metals (Basel). 6 (2016) 50. doi:10.3390/met6030050.

[5] A. Wolfenden, J.M. Wolla, Mechanical damping and dynamic modulus measurements in alumina and Tungsten fiber-reinforced aluminum composites, J. Mater. Sci. 24 (1989) 3205–3212.

[6] J.I. Rojas, A. Aguiar, D. Crespo, Effect of temperature and frequency of dynamic loading in the viscoelastic properties of aluminium alloy 7075-T6, Phys. Status Solidi C. 8 (2011) 3111–3114. doi:10.1002/pssc.201000732.

[7] J.I. Rojas, D. Crespo, Modeling of the effect of temperature, frequency and phase transformations on the viscoelastic properties of AA 7075-T6 and AA 2024-T3

aluminum alloys, Metall. Mater. Trans. A. 43 (2012) 4633–4646. doi:10.1007/s11661-012-1281-7.

[8] T. Das, S. Bandyopadhyay, S. Blairs, DSC and DMA studies of particulate-reinforced metal-matrix composites, J. Mater. Sci. 29 (1994) 5680–5688.

[9] A.S. Nowick, B.S. Berry, Anelastic Relaxation in Crystalline Solids, Academic Press, New York; London, 1972.

[10] D.W. Suh, R.H. Dauskardt, Mechanical relaxation time scales in a Zr-Ti-Ni-Cu-Be bulk metallic glass, J. Mater. Res. 17 (2002) 1254–1257.

[11] C. Liu, E. Pineda, D. Crespo, Mechanical relaxation of metallic glasses: An overview of experimental data and theoretical models, Metals (Basel). 5 (2015) 1073–1111. doi:10.3390/met5021073.

[12] S.B. Venkata Siva, Preparation and Characterization of Alumimium Metal Matrix Composite with Novel in situ Ceramic Composite Particles, Developed from Waste Colliery Shale Material, Acharya Nagarjuna University, 2015.

[13] J.I. Rojas, J. Nicolás, D. Crespo, Study on Mechanical Relaxations of 7075 (Al–Zn–Mg) and 2024 (Al–Cu–Mg) Alloys by Application of the Time-Temperature Superposition Principle, Adv. Mater. Sci. Eng. (2017). doi:10.1155/2017/2602953.

[14] A. Yousefiani, F.A. Mohamed, J.C. Earthman, Creep rupture mechanisms in annealed and overheated 7075 Al under multiaxial stress states, Metall. Mater. Trans. A-Physical Metall. Mater. Sci. 31A (2000) 2807–2821.

[15] I.S. Golovin, A. V Mikhaylovskaya, H. Sinning, Role of the β-phase in grain boundary and dislocation anelasticity in binary Al–Mg alloys, J. Alloys Compd. 577 (2013) 622–632. doi:10.1016/j.jallcom.2013.06.138.

[16] M. Yamaguchi, J. Bernhardt, K. Faerstein, D. Shtansky, Y. Bando, I.S. Golovin, H.-R. Sinning, D. Golberg, Fabrication and characteristics of melt-spun Al ribbons reinforced with nano/micro-BN phases, Acta Mater. 61 (2013) 7604–7615. doi:10.1016/j.actamat.2013.08.062.

[17] S. Belhas, A. Riviere, J. Woirgard, J. Vergnol, J. Defouquet, High-temperature relaxation mechanisms in Cu-Al solid-solutions, J. Phys. 46 (1985) 367–370.

[18] A. Riviere, M. Gerland, V. Pelosin, Influence of dislocation networks on the relaxation peaks at intermediate temperature in pure metals and metallic alloys, Mater. Sci. Eng. A-Structural Mater. Prop. Microstruct. Process. 521–22 (2009) 94–97. doi:10.1016/j.msea.2008.09.100 ER.

[19] E. Pineda, P. Bruna, B. Ruta, M. Gonzalez-Silveira, D. Crespo, Relaxation of rapidly

quenched metallic glasses: Effect of the relaxation state on the slow low temperature dynamics, Acta Mater. 61 (2013) 3002–3011. doi:10.1016/j.actamat.2013.01.060.

[20] M. Amiri, M.M. Khonsari, Life prediction of metals undergoing fatigue load based on temperature evolution, Mater. Sci. Eng. A-Structural Mater. Prop. Microstruct. Process. 527 (2010) 1555–1559. doi:10.1016/j.msea.2009.10.025.

[21] G.N. Hassold, E.A. Holm, D.J. Srolovitz, Effects of particle size on inhibited grain growth, Scr. Metall. Mater. 24 (1990) 101–106. doi:10.1016/0956-716X(90)90574-Z.

[22] P.R. Rios, G.S. Fonseca, Grain boundary pinning by Al6 Mn precipitates in an Al–1wt%Mn alloy, Scr. Mater. 50 (2004) 71–75. doi:10.1016/j.scriptamat.2003.09.031.

The highlights of this manuscript can be briefly stated as follows:

- the AMC is stiffer (shows higher storage modulus) than the A356 alloy matrix
- the AMC is most stable: a rapid stiffness decrease starts at higher temperature
- the AMC does not show relaxation peak in Al attributed to grain boundary sliding
- the AMC shows higher loss modulus and mechanical damping than the A356 alloy matrix
- due to relaxations related to reinforcement and larger grain size of alloy matrix